Atmos. Chem. Phys. Discuss., 15, 34913–34948, 2015
www.atmos-chem-phys-discuss.net/15/34913/2015/
doi:10.5194/acpd-15-34913-2015

Atmospheric Chemistry and Physics Discussions
Open Access

Rapid growth in nitrogen dioxide pollution over Western China, 2005–2013

Y.-Z. Cui[1], J.-T. Lin[2], C. Song[3], M.-Y. Liu[2], Y.-Y. Yan[2], Y. Xu[1], and B. Huang[1,4]

[1]Department of Geography and Resource Management, The Chinese University of Hong Kong, Shatin, NT, Hong Kong
[2]Laboratory for Climate and Ocean–Atmosphere Studies, Department of Atmospheric and Oceanic Sciences, School of Physics, Peking University, Beijing 100871, China
[3]Department of Geography, University of California, Los Angeles, Portola Plaza, Los Angeles, CA 90095, USA
[4]Institute of Space and Earth Information Science, The Chinese University of Hong Kong, Shatin, NT, Hong Kong

Received: 7 November 2015 – Accepted: 2 December 2015 – Published: 14 December 2015

Correspondence to: J.-T. Lin (linjt@pku.edu.cn) and B. Huang (bohuang@cuhk.edu.hk)

Published by Copernicus Publications on behalf of the European Geosciences Union.

Abstract

Western China has experienced rapid industrialization and urbanization since the implementation of the National Western Development Strategies (the "Go West" movement) in 1999. This transition has affected the spatial and temporal characteristics of nitrogen dioxide (NO_2) pollution. In this study, we analyze the trends and variability of tropospheric NO_2 vertical column densities (VCDs) from 2005 to 2013 over Western China, based on a wavelet analysis on monthly mean NO_2 data derived from the Ozone Monitoring Instrument (OMI) measurements. We focus on the anthropogenic NO_2 by subtracting region-specific "background" values dominated by natural sources. We find significant NO_2 growth over Western China between 2005 and 2013 ($8.6 \pm 0.9\,\%\,\mathrm{yr}^{-1}$ on average, relative to 2005), with the largest increments ($15\,\%\,\mathrm{yr}^{-1}$ or more) over parts of several city clusters. The NO_2 pollution in most provincial regions rose rapidly from 2005 to 2011 but stabilized or declined afterwards. The NO_2 trends were driven mainly by changes in anthropogenic emissions, as confirmed by a nested GEOS-Chem model simulation and a comparison with Chinese official emission statistics. The rate of NO_2 growth during 2005–2013 reaches $11.3 \pm 1.0\,\%\,\mathrm{yr}^{-1}$ over Northwestern China, exceeding the rates over Southwestern China ($5.9 \pm 0.6\,\%\,\mathrm{yr}^{-1}$) and the three well-known polluted regions in the east ($5.3 \pm 0.8\,\%\,\mathrm{yr}^{-1}$ over Beijing–Tianjin–Hebei, $4.0 \pm 0.6\,\%\,\mathrm{yr}^{-1}$ over the Yangtze River Delta, and $-3.3 \pm 0.3\,\%\,\mathrm{yr}^{-1}$ over the Pearl River Delta). Additional socioeconomic analyses suggest that the rapid NO_2 growth in Northwestern China is likely related to the fast developing resource- and pollution-intensive industries along with the "Go West" movement as well as relatively weak emission controls. Further efforts should be made to alleviate NO_x pollution to achieve sustainable development in Western China.

1 Introduction

Nitrogen oxides ($NO_x = NO + NO_2$) are major constituents in tropospheric chemistry, leading to ozone formation, acid deposition, and particulate matter pollution. NO_x are emitted into the troposphere from anthropogenic activities (thermal power plants, transportation, industries, and residential use) and natural sources (lightning, open fires, and soil) (Lin, 2012; Russell et al., 2012). Rapid economic development and urbanization across China in recent decades have caused serious air pollution problems, with NO_x becoming the fastest growing air pollutant in China over the last two decades (Richter et al., 2005; Zhang et al., 2012; Zhao et al., 2013).

Vertical column densities (VCDs) of tropospheric NO_2 retrieved from various satellite instruments have been used widely to study NO_x pollution over China (Richter et al., 2005; van der A et al., 2006; He et al., 2007; Wang et al., 2007b; Zhang et al., 2007b, 2012; Gu et al., 2013; Huang et al., 2013; J.-T. Lin et al., 2014). Satellite observations provide a tool to infer patterns of anthropogenic and natural NO_x emissions (Zhang et al., 2007a, 2009b; Stavrakou et al., 2008; van der A et al., 2008; Zhao and Wang, 2009; Li et al., 2010; Lin et al., 2010, 2015; Lamsal et al., 2011; Lin, 2012; Wang et al., 2012; Reuter et al., 2014). They are also useful to analyze the large variations in NO_x pollution during several short-term socioeconomic events, such as the Sino-African summit, Beijing Olympic Games, Shanghai Expo, Guangzhou Asian Games, Chinese economic recession and Chinese New Year (Wang et al., 2007a, 2009; Mijling et al., 2009; Witte et al., 2009; Hao et al., 2011; Lin and McElroy, 2011; Lin et al., 2013).

Most of prior studies have focused on Eastern China, with little attention paid to Western China. As shown in Fig. 1, Western China is specified here as the vast region covering six provinces (Gansu, Guizhou, Qinghai, Shaanxi, Sichuan and Yunnan), five provincial-level autonomous regions (Guangxi, Inner Mongolia, Ningxia, Tibet and Xinjiang), and one provincial-level municipality (Chongqing City). Western China has experienced significant socioeconomic changes following the National Western Development Strategies (the “Go West” movement) launched by the Chinese government in 1999. Over the last decade, the rates of industrialization and urbanization in Western China has accelerated (Deng and Bai, 2014). Western China is rich in natural resources, such as water, coal, natural gas, petroleum, and minerals. With the adjustment of regional development strategy at a national level, those energy-intensive industries formerly located in Eastern China have been encouraged to move westward, although the ecosystems of Western China may be more fragile than those of Eastern China (Shuai and Zhongying, 2008; Chen et al., 2010; Bai et al., 2014). Although the "Go West" movement is beneficial for local industrial and economic development in Western China, it may have led to unintended environmental impacts that have yet to be understood. The short lifetime of tropospheric NO_2 (hours to a day), its strong link and rapid response to emissions, and the availability of high-quality satellite measurements allow to evaluating pollution changes and the possibility of sustainable development in Western China. Satellite measurements are particularly important in lack of sufficient ground-based measurements.

This study investigates the spatiotemporal variations of tropospheric NO_2 VCDs between October 2004 and May 2014 over Western China and potential human influences, by analyzing the monthly Royal Netherlands Meteorological Institute (KNMI) Ozone Monitoring Instrument (OMI) NO_2 data (DOMINO v2). We apply a wavelet decomposition analysis to reveal the long-term trends and seasonal variation of tropospheric NO_2 over Western China. We also use a nested GEOS-Chem simulation and Chinese official emission statistics to confirm that anthropogenic emissions are the main driver of NO_2 variations. At last, we discuss the regional differences in NO_2 growths between Northwestern and Southwestern China and between Western and Eastern China, and we associate these differences with the driving socioeconomic factors of individual regions.

2 Data and study area

2.1 Satellite data

OMI is onboard the EOS-Aura satellite. The satellite measurements have a pixel size of 13 km × 24 km at nadir with a local overpass time around 13:40. VCDs of tropospheric NO_2 are derived in three major steps, including derivation of slant column densities (SCDs), separation of stratospheric and tropospheric SCDs, and calculation of tropospheric air mass factors (AMFs) for deduction of the tropospheric VCDs. On a regional and monthly mean basis, the relative error of retrieved VCDs is about $30\,\% + 0.7 \times 10^{15}$ molecules cm^{-2} (Boersma et al., 2011; Lin and McElroy, 2011). More detailed algorithms and error descriptions involved in retrieving tropospheric NO_2 VCDs can be found in Boersma et al. (2007, 2011).

We mapped the level-2 DOMINO v2 product (http://www.temis.nl/airpollution/no2.html) to a 0.25° × 0.25° grid, and then averaged daily data to produce monthly mean VCD values. We used data from October 2004 to May 2014 for the present analysis. For data quality control, we excluded pixels with a cloud radiance fraction $> 50\,\%$ or affected by row anomaly (Boersma et al., 2011). We filled the missing monthly mean values in some grid cells using values in the adjacent years; the impact on the trend analysis is found to be small by sensitivity analyses on the respective GEOS-Chem simulation results (see Sect. 4.2).

2.2 GEOS-Chem modeling

We used the nested GEOS-Chem chemical transport model version 9-02, on a 0.667° long. ×0.5° lat. grid with 47 vertical layers, to simulate the tropospheric NO_2 and other pollutants over Asia (Chen et al., 2009). The model is run with the full O_x-NO_x-VOC-CO-HO_x gaseous chemistry and online aerosol calculations, and it is driven by the GEOS-5 assimilated meteorology from the NASA Global Modeling and Assimilation Office. Vertical mixing in the planetary boundary layer follows the non-local parameterization scheme implemented by (Lin et al., 2010). Convection is simulated with a modified Relaxed Arakawa–Schubert scheme (Rienecker et al., 2008). Lateral boundary conditions of the nested model are updated every 3 h by results from corresponding global modeling on a 5° long. ×4° lat. grid.

Chinese anthropogenic emissions of NO_x and other species adopt the monthly MEIC inventory with a base year of 2008 (www.meicmodel.org). We further scaled monthly anthropogenic NO_x emissions to other years, by applying the ratios of monthly DOMINO v2 NO_2 VCDs in those years over the VCDs in the respective months of 2008. Emissions for other Asian regions follow the INTEX-B inventory (Zhang et al., 2009a). Other model setups are referred to Lin et al. (2015).

Due to limited meteorological inputs, model simulations were conducted from 2004 to April 2013. The first simulation year was used for model spin-up, and results from 2005 onward were analyzed in the present analysis. Modeled vertical profiles of NO_2 were averaged over 13:00–15:00 local time, regridded to a $0.25° \times 0.25°$ grid, applied with the DOMINO averaging kernel (AK), sampled in locations and days with valid OMI data, and then averaged to derive monthly mean VCDs values. The use of AK was to eliminate the effect of differences in NO_2 vertical profiles between GEOS-Chem and TM4 (that provides the priori profiles for the DOMINO retrieval). Modeled VCDs data without applying the AK are also analyzed in Sect. 4.2 to test the effects of data sampling and temporal interpolation.

2.3 Official anthropogenic emission and socioeconomic data

We took Chinese official provincial-level NO_x emission inventory for 2007 and 2010–2013 to compare with trends in OMI NO_2. Chinese central government commenced its official estimate of anthropogenic NO_x emissions following the first nationwide pollution census in 2007 (The first nationwide pollution census committee, 2011). NO_x emissions in 2010–2013 were also based on the estimating system of the first pollution census, allowing for a consistent comparison throughout time. We also included the official emission targets aimed for 2015 from the 12th Five-Year Plan (2011–2015), a well-known socioeconomic planning step of China. We obtained all socioeconomic data from the China Statistical Yearbooks Database (http://tongji.cnki.net/overseas/engnavi/navidefault.aspx).

2.4 Study area

Figure 1 highlights the study area in China. We extracted provincial and regional NO_2 data according to their administrative divisions. We separated Western China into two sub-regions, including Northwestern China (Gansu, Inner Mongolia, Ningxia, Qinghai, Shaanxi and Xinjiang) and Southwestern China (Chongqing, Guangxi, Guizhou, Sichuan and Yunnan). Tibet is excluded from the present analysis due to lack of socioeconomic data. We also selected three key regions from Eastern China for comparisons with Western China: the Beijing-Tianjin-Hebei region (BTH, including Beijing, Tianjin and Hebei Province), the Yangtze River Delta (YRD, including Shanghai, Jiangsu Province and Zhejiang Province) and the Pearl River Delta (PRD, part of Guangdong Province).

3 Methods

3.1 Removing contributions from natural sources

This study is focused on areas that have been subjected to significant changes in anthropogenic NO_x emissions. Since NO_x are emitted from both anthropogenic and natural sources (Lin, 2012), we removed the natural contributions by taking advantage of their distinctive seasonal patterns. Over China, anthropogenic emissions tend to maximize in winter, although the seasonal variation is often within 20 % (Zhang et al., 2009a). Soil and lightning emissions exhibit summer maxima with very low values in winter. Biomass burning emissions of NO_x are negligible over China (Lin, 2012). In addition, the lifetime of NO_x in winter is several times longer than in summer. Therefore the NO_2 VCDs are the lowest in summer and the highest in winter over the areas dominated by anthropogenic sources, while the opposite seasonality occurs over the regions dominated by natural emissions (Lin, 2012). Furthermore, lightning and soil emissions are mostly independent of direct anthropogenic influences for 2005–2013, albeit with certain effects from changes in climate and/or land use. There is no evidence that these natural emissions underwent significant trends from 2005 to 2013. By comparison, anthropogenic emissions have exhibited dramatic changes along with the rapid socioeconomic development, and these changes have affected the seasonality of NO_2.

Figure 2a shows the seasonal variation in OMI NO_2 VCDs, averaged over 2005–2013, for each 0.25° × 0.25° grid cell in Western China; the grid cells are ordered according to their 9 year mean NO_2 values. Once a grid cell is ordered, its 9 year mean monthly NO_2 values are converted to their reverse ranks (from 1 to 12) in the 12 month dataset. Figure 2a shows that for grid cells with 9 year mean NO_2 VCDs below 1.0×10^{15} molecules cm^{-2}, NO_2 generally experiences summer maxima and winter minima, reflecting the dominance of natural sources. In contrast, grid cells with 9 year mean NO_2 VCDs above 1.0×10^{15} molecules cm^{-2} exhibit winter maxima, due to the dominance of anthropogenic emissions as well as a longer lifetime.

Figure 2b further shows the standard deviation (SD) of monthly OMI NO_2 VCDs year by year for each 0.25° × 0.25° grid cell in Western China; the grid cells are ordered according to their 9 year mean NO_2 values. Once a grid cell is ordered, its SD values are converted to their reverse ranks (from 1 to 9) in the 9 year dataset. Figure 2b shows that grid cells with 9 year mean NO_2 VCDs above 1.0×10^{15} molecules cm^{-2} exhibit a large growth in SD especially since 2009, as a result of large growth in anthropogenic emissions that amplified the seasonality. By comparison, grid cells with 9 year mean NO_2 VCDs below 1.0×10^{15} molecules cm^{-2} did not experience such significant changes in SD between 2005 and 2013.

Based on the above seasonality analysis, we determined the regions dominated by anthropogenic emissions as those with 2005–2013 mean NO_2 VCDs exceeding 1.0×10^{15} molecules cm^{-2}. To further remove natural influences, we identified six “back-

Title Page
Abstract | Introduction
Conclusions | References
Tables | Figures
◀| |▶
◀ ▶
Back | Close
Full Screen / Esc
Printer-friendly Version
Interactive Discussion

ground" areas that are away from cities and are supposed to be dominated by natural emissions (see the hatched areas in Fig. 1), a method similar to Russell et al. (2012). The "background" regions in Western China are normally the uninhabited areas with very low 9 year mean NO_2 VCDs (0.4–0.5×10^{15} molecules cm^{-2}, much lower than in the polluted areas, Table 1). The "background" regions in Eastern China have higher NO_2 values, at 0.7–1.2×10^{15} molecules cm^{-2}; however, these values are still several times lower than the values in the polluted eastern regions (Table 1). When calculating the trends and seasonal variation of NO_2 in the grid cells of the chosen human-dominant areas, we subtracted NO_2 VCDs at these grid cells by the NO_2 value averaged over the nearest "background" region. The subtraction was done on a monthly basis. We processed the model NO_2 data with the same method. Note that the "background" regions may not be totally free from anthropogenic influences, as certain amount of NO_x in the polluted areas may be oxidized to produce peroxyacyl nitrates (PANs), which can be transported to "background" areas and converted back to NO_x. The effect of this residual anthropogenic NO_x on our trend analysis is small, since the NO_2 values over the "background" regions are much lower than over the polluted areas.

3.2 Wavelet decomposition analysis

Due in part to the short lifetime of NO_x, the tropospheric NO_2 concentrations respond quickly to emission changes at various temporal scales, from a general growth along with socioeconomic development to short-term perturbations such as the Chinese New Year holidays and the economic recession (Lin and McElroy, 2011; Lin et al., 2013). We thus conducted discrete wavelet transform (DWT) to distinguish temporal variability of NO_2 at multiple scales (Pišoft et al., 2004; Partal and Küçük, 2006; Nalley et al., 2012). The multi-scale analysis in DTW is able to decompose a time series $f(t)$ into n-scale components (n is the decomposition level):

$$f(t) = \sum_{i=1}^{n} \mathrm{D}_i + \mathrm{A}_n \quad (1)$$

where D_i is a detailed signal (high frequency) at level i and A_n is the approximate signal (low frequency) at the set of maximum level n. The detailed and approximate coefficients were produced by convolution of time series with wavelet functions and scaling functions. Then both coefficients were reconstructed to have the same temporal length as the original signal (Nalley et al., 2012).

We chose Discrete Meyer (dmey) as the basis function with a wavelet decomposition number of five. The decomposition number is normally the number of data after last subsampling, and it is smaller than the function length (de Artigas et al., 2006). Increasing the decomposition level leads to smoother results for detailed and approximate signals at the compensation of increased estimate errors (Chou, 2011). We tested the decomposition number n from 3 to 7 and selected a number at 5 that separates the trends and seasonality from smaller timescales. As a result, the approximate signal $A5$ represents the long-term trend of the original NO_2 time series, and the detailed components $D1$–$D5$ indicate higher-frequency variations. In particular, $D3$ reflects the seasonal variation with a period of about 12 months. As an example, Fig. 3 presents the wavelet transform result for one grid cell (34.5° N, 108.9° E, in Xi'an City). Note that our wavelet decomposition does not require prior assumptions on seasonality and other temporal scales, different from the approaches adopted by previous NO_2 studies (e.g.,van der A et al., 2006).

4 Results and analysis

4.1 Spatial patterns of tropospheric NO_2 VCDs over China

Figure 4 shows the spatial distributions of annual average OMI NO_2 VCDs over China in 2005, 2012 and 2013. Here the "background" values have not been subtracted. The NO_2 VCDs exceed a high value of 6×10^{15} molecules cm^{-2} in many areas of Central-East China and parts of Western China. Chengdu-Chongqing, Urumqi and Shaanxi-Guanzhong city clusters are well-known pollution "hot spots" of Western China (see

Fig. 1 for region definitions). These “hot spots” have intensified since 2005, as well as other polluted western areas including Gansu-Ningxia and Inner Mongolia industrial city clusters. The annual and regional average NO_2 VCDs over Western China has increased by 51 % between 2005 and 2013, higher than the increase at 41 % in Central-East China. The large growth of NO_2 over Western China highlights the necessity of understanding potential human influences in these regions.

Figure 4 also compares the OMI derived and GEOS-Chem modeled annual average NO_2 VCDs in 2005 and 2012. OMI and model NO_2 share similar spatial and temporal patterns. Linear regression for model NO_2 as a function of OMI NO_2 reveals that for a given year, model NO_2 are highly correlated with OMI values in space (R^2 is around 0.90; see Fig. 4 for a scatterplot for 2012 and Table 2 for statistics for other years). Table 2 shows that for 2008, the magnitudes of model NO_2 are also close to OMI NO_2 (slope = 1.09). For other years, the slopes are larger (1.11–1.26), indicating positive model biases. The biases reflect the nonlinear relation between changes in NO_x emissions and changes in NO_2 VCDs (Martin et al., 2003; Valin et al., 2011; Lin, 2012) that we did not account for when linearly scaling model emissions from MEIC 2008 to other years based on the interannual variation in OMI NO_2.

4.2 Trends and seasonal variation of NO_2 over Western China

Figure 5 shows OMI and modeled NO_2 trends at individual grid cells over Western China, by applying a linear regression to the approximate signal *A5* from the wavelet decomposition. All trend values are normalized relative to the 2005 mean NO_2 VCDs. All the NO_2 data have been subtracted by its respective “background” values prior to the wavelet analysis. Results are only shown for grid cells with 2005–2013 average NO_2 VCDs exceeding 1.0×10^{15} molecules cm^{-2} and with statistically significant trends (P value < 0.05 according to an F test).

Figure 5a shows that OMI NO_2 grew at most grid cells from 2005 to 2013, with a regional average annual growth at $8.6 \pm 0.9\,\%\,\mathrm{yr}^{-1}$. NO_2 grew the fastest over the city clusters, reflecting rapid economic development, urbanization, and population growth. Parts of Chengdu-Chongqing, Shaanxi-Guanzhong and Urumqi city clusters experienced NO_2 growth of 15 % yr^{-1} or more. Most grid cells in yellow color are suburban or rural areas, but they also underwent rapid NO_2 growth since 2005 (6–10 % yr^{-1}).

A comparison of Fig. 5b and c shows that GEOS-Chem generally captures the OMI NO_2 trends from 2005 to 2012, suggesting that anthropogenic emissions are the main driver of the observed NO_2 trend. OMI data exhibit a stronger growth than modeled data over North Xinjiang, East and South Inner Mongolia, South Sichuan, East Guizhou and South Guangxi, whereas the OMI trends are weaker than the modeled trends over most of other regions. The differences between modeled and OMI NO_2 reflect the strong but nonlinear relation between NO_x emissions and NO_2 VCDs.

Table 1 shows the trends of OMI NO_2 VCDs from 2005 to 2013, as a percentage of mean values in 2005, on a provincial basis. NO_2 grew the fastest over Xinjiang, Ningxia and Qinghai with a growth rate at 15.1, 12.3 and 11.2 % per year, respectively. The growth rates in Northwestern China (7.5–15.1 % yr^{-1}) were much greater than the rates in Southwestern China (4.0–7.8 % yr^{-1}), primarily as a result of the regional differences in socioeconomic development (see Sect. 5.2).

Figure 6 further shows the *A5* monthly time series for individual provinces as a result of wavelet analyses on OMI NO_2. All values are normalized with respect to 2005. In particular, the OMI_1 time series (black line) results from a wavelet analysis on OMI NO_2 over October 2004–May 2014. OMI_1 shows that NO_2 grew rapidly between 2007 and 2011 over all provinces. For Xinjiang, Qinghai and Yunnan, OMI NO_2 increased continuously from 2005 to 2013. Over other provinces, OMI NO_2 peaked around 2011–2012 and then stagnated or even slightly declined thereafter. These stagnation or reduction patterns likely reflect recent effective emission control policies (see Sect. 5.1).

Figure 6 also compares the *A5* time series for OMI NO_2 (OMI_2, green line) and model NO_2 (GC_AK, red line) derived from wavelet analyses on the same time period from January 2005 to April 2013. Model results were sampled coincidently with OMI data and were applied with the AK. OMI_2 and GC_AK do not show a stagnation/reduction feature as obvious as OMI_1 after 2011, because of a shorter time series for wavelet decomposition. OMI_2 and GC_AK exhibit similar increasing trends and variability in most western provinces, confirming that variations in anthropogenic emissions (accounted for in the model) were the main driver of NO_2 changes.

Our trend analyses may be affected by missing OMI data and the corresponding temporal interpolation procedure. To evaluate the effects, we compared two additional datasets based on model results: GC_NAK1 (blue line in Fig. 6) represents model NO_2 in all days without applying the AK, and GC_NAK2 (orange line) represents model NO_2 sampled from days with valid OMI data but without applying the AK. Figure 6 shows almost no differences between GC_NAK1 and GC_NAK2 for all provinces. Therefore the missing data have little influence on our trend analyses.

Figure 7 shows the seasonal variation of provincial mean OMI NO_2, as represented by the *D3* component from the wavelet analysis. The dominant anthropogenic emissions have resulted in winter NO_2 maxima and summer minima. The NO_2 seasonality increased from 2005 to 2011/12 and decreased afterwards. The strength of seasonality, in terms of absolute VCD values, varied by a factor of about six along with changes in annual mean NO_2 levels, revealing the rapidly changing anthropogenic influences. The changes in NO_2 seasonality mainly reflects a larger absolute increase in wintertime NO_2 VCD (due to a longer lifetime) than in summertime for a given amount of emission increase. Also, an increase in emissions enhances the NO_x lifetime in winter but with a reduction in summer (Lin and McElroy, 2011).

4.3 Comparison between satellite observations and bottom-up emission estimates

Figure 8 shows Chinese official bottom-up provincial anthropogenic emission inventory for 2007 and 2010–2013, together with the provincial emission targets for 2015 (as a goal of the 12th Five-Year Plan) (The State Council of the People's Republic of China, 2011a). Provincial mean OMI NO_2 VCDs are also shown for comparison. Both emission and VCD datasets were normalized to their 2007 mean values to remove the effect of regional dependence in the relation between NO_x emissions and NO_2 VCDs. Ningxia, Xinjiang and Inner Mongolia had the largest increases in NO_x emissions from 2007 to 2010, consistent with their growth of NO_2 VCDs. NO_x emissions in most provinces grew significantly from 2007 to 2010 and peaked in 2011–2012, also in general consistency with the trends in OMI NO_2. On the other hand, the emission inventory suggests a reduction since 2011 for Xinjiang and Yunnan, inconsistent with the notable growth in NO_2 VCDs. This likely suggests an underestimate in the official emission inventory.

5 Relating pollution changes to socioeconomic development and environmental policies

5.1 General discussion on NO_2 trends over Western China

As described in Sect. 4, the tropospheric NO_2 VCDs over Western China have grown notably since 2005. The growth occurred not only over cities but also over many suburban and rural regions, indicating an expansion of human influences from urban to remote areas. This scale of pollution growth was associated with the rapid urbanization and industrialization over Western China following the "Go West" movement. Table 3 shows that the urban population (i.e., the percentage of total population living in urban areas) increased by 10 % or more from 2005 to 2013 in all provinces of Western China except Xinjiang. Over the same period, Western China experienced steep economic growth with industrial GDP growth rates of 12.4–20.3 % yr^{-1} across the provinces.

On the other hand, the NO_2 VCDs declined or stabilized since 2011 in many provinces (see Fig. 7), partly reflecting some improvements in environmental strategies. China's air pollution control strategy has been transformed from a traditional end–of–pipe control strategy (i.e., only using low NO_x combustion technologies in some power plants) into a combined energy saving and emission reduction strategy after 2006 (Gu et al., 2013; Zhao et al., 2013). In particular, total NO_x emissions have become a major target of national pollution control in the 12th Five-Year Plan (2011–2015), with a legally binding goal to reduce the national emissions by nearly 10 % in 2015 compared to 2010 (The State Council of the People's Republic of China, 2011b). Furthermore, Chinese central government has also decided to consider the effectiveness of this reduction in evaluating local governments' performance (The State Council of the People's Republic of China, 2012). In aspect of energy saving measures, great efforts have also been made to improve energy efficiency, to slow down growth of energy demand, and to adjust structure in various sectors (power plants, transportation, industries, and residential use) over the past few years (Wang and Hao, 2012; Zhao et al., 2013).

5.2 On the contrast between Northwestern and Southwestern China

Northwestern China (Inner Mongolia, Xinjiang, Qinghai, Gansu and Shaanxi) has an average NO_2 growth rate at $11.3 \pm 1.0\,\%\,\mathrm{yr}^{-1}$ from 2005 to 2013, about twice the average growth rate ($5.9 \pm 0.6\,\%\,\mathrm{yr}^{-1}$) in Southwestern China (Sichuan, Chongqing, Guizhou, Guangxi and Yunnan). The contrast in NO_2 growth rate between Northwest and Southwest reflects their distinctive states of socioeconomic development. According to the nationwide pollution census, Northwestern China generates much more NO_x emissions per unit of GDP (11.94 tonnes/billion RMB in 2007) than the Southwest (6.98 tonnes/billion RMB) (The first nationwide pollution census committee, 2011). The difference in pollution intensities also reflects their dissimilar economic structures. In particular, Northwestern China has recently become an important energy producer (due to the "West to East Power Transmission" project) and a heavy industry base (in terms of mining, fossil fuels and raw materials) (Chen et al., 2010; Deng and Bai, 2014), and these industries are often associated with significant NO_x emissions. The electricity consumption of heavy industries in Northwestern China grew by 152.5 % from 2005 to 2011, greater than the growth at 99.6 % in Southwestern China.

About 70 % of China's industrial and residential energy consumption is supplied by coal burning in 2009 (Li and Leung, 2012), and the value has not changed drastically in later years. Figure 9 shows that Northwestern China has consumed more coal than the Southwest since 2005, and by 2012 their difference has increased by a factor of 35 (from merely 9.03 million tonnes in 2005 to as large as 318.3 million tonnes in 2012). For the Northwest, there is extremely high correlation between NO_2 VCDs and coal use across the years ($R^2 = 0.95$, P value < 0.05), compared to a correlation at 0.84 (P value < 0.05) for the Southwest.

Furthermore, the annual amount of electricity generated by coal-fired power plants in Northwestern China increased by 237 %, from 226.3 billion kWh in 2005 to 763.1 billion kWh in 2013; the annual growth rates are 9.8–22.8 $\%\,yr^{-1}$ for individual provinces (see Table 3). The growth was smaller in the Southwest, about 110 % from 165.6 to 347.9 billion kWh, translated to growth rates of 6.0–14.9 $\%\,yr^{-1}$ for individual provinces. This difference was partly due to the stronger growth in hydropower production in the Southwest (from 147.2 to 471.6 billion kWh over 2005–2013, at the rates of 8.9–21.6 $\%\,yr^{-1}$ in individual provinces) than the growth in the Northwest (from 40.0 to 107.3 billion kWh, 4.7–18.4 $\%\,yr^{-1}$).

Transportation plays a more important role in NO_x pollution over the Southwest, comparing with the Northwest. Table 3 shows that transportation contributes to much larger fractions of NO_x emissions in the capital cities of Southwestern China than in the Northwestern capital cities except Xi'an, Shaanxi. In addition, the number of vehicles grew faster in the Southwestern capital cities during 2005–2012.

5.3 On the contrast between Western and Eastern China

The average growth rate was $8.6 \pm 0.9\,\%\,yr^{-1}$ for Western China, much larger than the rates in the three key eastern regions BTH ($5.3 \pm 0.8\,\%\,yr^{-1}$), YRD ($4.0 \pm 0.6\,\%\,yr^{-1}$) and PRD ($-3.3 \pm 0.3\,\%\,yr^{-1}$) (see Table 1). This regional contrast reflects both their economic activities and the emission control policies adopted by the Chinese central and local governments. In particular, China's development strategy for its western provinces might have led to unintended westward pollution migration, as many resource- and pollution-intensive industries gradually moved from the East to the West after 2000. Table 3 shows that from 2005 to 2013, the average industrial GDP growth rate in Western China was 17.2 % yr^{-1} (relative to 2005), higher than the rates in the three key eastern regions (13.2 % yr^{-1} in BTH, 11.6 % yr^{-1} in YRD and 12.0 % yr^{-1} in PRD). The fast economic and pollution growth in Western China in part reflects its growing production to support consumption in other regions (J. Lin et al., 2014; Zhao et al., 2015). According to Zhao et al. (2015), NO_x emissions over Western China in 2007 were largely attributable to the economic production to supply Eastern China and foreign countries, with 366 Gg related to interprovincial trade and 49.1 Gg related to international trade. Together with atmospheric transport, trade has become a critical mechanism for transboundary pollution transfer at both the global and regional scales (Lin, J. et al., 2014), with significant consequences on public health (Jiang et al., 2015).

The west-east contrast in NO_2 growth also reflected their different pollution control strategies and measures. Although China has a national NO_x emission reduction target at 10 % (from 2010 to 2015), the targets are set differently for individual provinces. Table 1 shows that the targets were higher, at 13.9, 17.7 and 16.9 %, for the three key eastern regions (BTH, YRD, and PRD), but they are as low as 5.7 % averaged over Western China (The State Council of the People's Republic of China, 2011a). In particular, an emission increase by 15 % is allowed for Qianghai Province. In addition, although NO_x emission reduction measures have been taken in power plants and some other industrial sectors since 2006 (via de-nitrification systems that involve selective catalytic or non-catalytic reduction), by 2010 as much as 57 % of these systems were installed in the three key eastern regions (Zhao et al., 2013). The capacity of small power generators being shut-down in Western China was about 10808 MW (excluding small diesel generators), only accounting for about 19 % of the capacity of total shut-down small power plants in China (55630 MW) during the 11th Five-Year Plan period (2006–2010) (NDRC, 2009–2011; Xu et al., 2013).

Furthermore, the vehicle emission control has also been implemented much more stringently in the East than in the West (Li and Leung, 2012). Although large amounts of "Yellow-Label Vehicles" (YLVs, highly-emitting vehicles that fail to meet the National

I emission standard) have been banned from entering into big cites in Eastern China, over the recent years a considerable number of used YLVs have been brought to the West that has much weaker restrictions on YLVs (Qi, 2010). Greater efforts to reduce NO_x pollution in Western China, with lessons learnt from the East, will help to achieve its sustainable development.

6 Conclusions

This study investigates the spatiotemporal variations of tropospheric NO_2 VCDs over Western China during 2005–2013, by using a wavelet decomposition analysis to distinguish long-term trends, seasonal variation and other scales of temporal variability. We focus on the anthropogenic NO_2 by subtracting region-specific "background" values dominated by natural sources. We find NO_2 grew rapidly over Western China at a regional average rate of $8.6 \pm 0.9\,\%\,\mathrm{yr}^{-1}$ from 2005 to 2013. Under the competing influences of economic growth and emission control, NO_2 levels in most western provinces increased from 2005 to 2011 and stabilized or slightly declined afterwards. GEOS-Chem model simulations and the official emission statistics are used to confirm that the OMI observed NO_2 trends were driven mainly by changes in anthropogenic emissions.

Between 2005 and 2013, Northwestern China experienced much larger NO_2 growth ($11.3 \pm 1.0\,\%\,\mathrm{yr}^{-1}$) than Southwestern China ($5.9 \pm 0.6\,\%\,\mathrm{yr}^{-1}$) and the three traditional key regions of Eastern China (BTH, YRD and PRD, -3.3 to $+5.3\,\%\,\mathrm{yr}^{-1}$). The rapid NO_2 growth in Northwestern China was possibly attributed to the fast developing resource- and pollution-intensive industries along with the "Go West" movement as well as relatively weak emission controls. Rapid industrialization and urbanization in Western China should be accompanied with more stringent pollution control to achieve sustainable development.

Acknowledgements. This research is supported by the National Natural Science Foundation of China, grant 41175127 and 41422502, and by the 973 program, grant 2014CB441303. We acknowledge the free use of DOMINO v2 NO_2 product from www.temis.nl.

References

Bai, X., Shi, P., and Liu, Y.: Realizing China's urban dream, Nature, 509, 158–160, doi:10.1038/509158a, 2014.

Boersma, K. F., Eskes, H. J., Veefkind, J. P., Brinksma, E. J., van der A, R. J., Sneep, M., van den Oord, G. H. J., Levelt, P. F., Stammes, P., Gleason, J. F., and Bucsela, E. J.: Near-real time retrieval of tropospheric NO_2 from OMI, Atmos. Chem. Phys., 7, 2103–2118, doi:10.5194/acp-7-2103-2007, 2007.

Boersma, K. F., Eskes, H. J., Dirksen, R. J., van der A, R. J., Veefkind, J. P., Stammes, P., Huijnen, V., Kleipool, Q. L., Sneep, M., Claas, J., Leitão, J., Richter, A., Zhou, Y., and Brunner, D.: An improved tropospheric NO_2 column retrieval algorithm for the Ozone Monitoring Instrument, Atmos. Meas. Tech., 4, 1905–1928, doi:10.5194/amt-4-1905-2011, 2011.

Chen, D., Wang, Y., McElroy, M. B., He, K., Yantosca, R. M., and Le Sager, P.: Regional CO pollution and export in China simulated by the high-resolution nested-grid GEOS-Chem model, Atmos. Chem. Phys., 9, 3825–3839, doi:10.5194/acp-9-3825-2009, 2009.

Chen, W., Li, H., and Wu, Z.: Western China energy development and west to east energy transfer: application of the Western China Sustainable Energy Development Model, Energ. Policy, 38, 7106–7120, doi:10.1016/j.enpol.2010.07.029, 2010.

Chou, C.-M.: Wavelet-based multi-scale entropy analysis of complex rainfall time series, Entropy, 13, 241, doi:10.3390/e13010241, 2011.

de Artigas, M. Z., Elias, A. G., and de Campra, P. F.: Discrete wavelet analysis to assess long-term trends in geomagnetic activity, Phys. Chem. Earth, 31, 77–80, doi:10.1016/j.pce.2005.03.009, 2006.

Deng, X. and Bai, X.: Sustainable Urbanization in Western China, Environment: Science and Policy for Sustainable Development, 56, 12–24, doi:10.1080/00139157.2014.901836, 2014.

Gu, D., Wang, Y., Smeltzer, C., and Liu, Z.: Reduction in NO_x emission trends over China: regional and seasonal variations, Environ. Sci. Technol., 47, 12912–12919, doi:10.1021/es401727e, 2013.

Hao, N., Valks, P., Loyola, D., Cheng, Y. F., and Zimmer, W.: Space-based measurements of air quality during the World Expo 2010 in Shanghai, Environ. Res. Lett., 6, 044004, doi:10.1088/1748-9326/6/4/044004, 2011.

He, Y., Uno, I., Wang, Z., Ohara, T., Sugimoto, N., Shimizu, A., Richter, A., and Burrows, J. P.: Variations of the increasing trend of tropospheric NO_2 over central east China during the past decade, Atmos. Environ., 41, 4865–4876, doi:10.1016/j.atmosenv.2007.02.009, 2007.

Huang, J., Zhou, C., Lee, X., Bao, Y., Zhao, X., Fung, J., Richter, A., Liu, X., and Zheng, Y.: The effects of rapid urbanization on the levels in tropospheric nitrogen dioxide and ozone over East China, Atmos. Environ., 77, 558–567, doi:10.1016/j.atmosenv.2013.05.030, 2013.

Jiang, X., Zhang, Q., Zhao, H., Geng, G., Peng, L., Guan, D., Kan, H., Huo, H., Lin, J., Brauer, M., Martin, R. V., and He, K.: Revealing the hidden health costs embodied in Chinese Exports, Environ. Sci. Technol., 49, 4381–4388, doi:10.1021/es506121s, 2015.

Lamsal, L. N., Martin, R. V., Padmanabhan, A., van Donkelaar, A., Zhang, Q., Sioris, C. E., Chance, K., Kurosu, T. P., and Newchurch, M. J.: Application of satellite observations for timely updates to global anthropogenic NO_x emission inventories, Geophys. Res. Lett., 38, L05810, doi:10.1029/2010GL046476, 2011.

Li, C., Zhang, Q., Krotkov, N. A., Streets, D. G., He, K., Tsay, S.-C., and Gleason, J. F.: Recent large reduction in sulfur dioxide emissions from Chinese power plants observed by the Ozone Monitoring Instrument, Geophys. Res. Lett., 37, L08807, doi:10.1029/2010GL042594, 2010.

Li, R. and Leung, G. C. K.: Coal consumption and economic growth in China, Energ. Policy, 40, 438–443, doi:10.1016/j.enpol.2011.10.034, 2012.

Lin, J., Pan, D., Davis, S. J., Zhang, Q., He, K., Wang, C., Streets, D. G., Wuebbles, D. J., and Guan, D.: China's international trade and air pollution in the United States, P. Natl. Acad. Sci. USA, 111, 1736–1741, doi:10.1073/pnas.1312860111, 2014.

Lin, J.-T.: Satellite constraint for emissions of nitrogen oxides from anthropogenic, lightning and soil sources over East China on a high-resolution grid, Atmos. Chem. Phys., 12, 2881–2898, doi:10.5194/acp-12-2881-2012, 2012.

Lin, J.-T. and McElroy, M. B.: Detection from space of a reduction in anthropogenic emissions of nitrogen oxides during the Chinese economic downturn, Atmos. Chem. Phys., 11, 8171–8188, doi:10.5194/acp-11-8171-2011, 2011.

Lin, J.-T., McElroy, M. B., and Boersma, K. F.: Constraint of anthropogenic NO_x emissions in China from different sectors: a new methodology using multiple satellite retrievals, Atmos. Chem. Phys., 10, 63–78, doi:10.5194/acp-10-63-2010, 2010.

Lin, J.-T., Pan, D., and Zhang, R.-X.: Trend and interannual variability of Chinese air pollution since 2000 in association with socioeconomic development: a brief overview, Atmos. Oceanic Sci. Lett., 6, 84–89, 2013.

Lin, J.-T., Martin, R. V., Boersma, K. F., Sneep, M., Stammes, P., Spurr, R., Wang, P., Van Roozendael, M., Clémer, K., and Irie, H.: Retrieving tropospheric nitrogen dioxide from the Ozone Monitoring Instrument: effects of aerosols, surface reflectance anisotropy, and vertical profile of nitrogen dioxide, Atmos. Chem. Phys., 14, 1441–1461, doi:10.5194/acp-14-1441-2014, 2014.

Lin, J.-T., Liu, M.-Y., Xin, J.-Y., Boersma, K. F., Spurr, R., Martin, R., and Zhang, Q.: Influence of aerosols and surface reflectance on satellite NO_2 retrieval: seasonal and spatial characteristics and implications for NO_x emission constraints, Atmos. Chem. Phys. Discuss., 15, 12653–12714, doi:10.5194/acpd-15-12653-2015, 2015.

Martin, R. V., Jacob, D. J., Chance, K., Kurosu, T. P., Palmer, P. I., and Evans, M. J.: Global inventory of nitrogen oxide emissions constrained by space-based observations of NO_2 columns, J. Geophys. Res.-Atmos., 108, 4537, doi:10.1029/2003JD003453, 2003.

Mijling, B., van der A, R. J., Boersma, K. F., Van Roozendael, M., De Smedt, I., and Kelder, H. M.: Reductions of NO_2 detected from space during the 2008 Beijing Olympic Games, Geophys. Res. Lett., 36, L13801, doi:10.1029/2009GL038943, 2009.

Nalley, D., Adamowski, J., and Khalil, B.: Using discrete wavelet transforms to analyze trends in streamflow and precipitation in Quebec and Ontario (1954–2008), J. Hydrol., 475, 204–228, doi:10.1016/j.jhydrol.2012.09.049, 2012.

NDRC: List of Decommissioned Small Thermal Power Plants, Beijing, China, 2009–2011.

Partal, T. and Küçük, M.: Long-term trend analysis using discrete wavelet components of annual precipitations measurements in Marmara region (Turkey), Phys. Chem. Earth, 31, 1189–1200, doi:10.1016/j.pce.2006.04.043, 2006.

Pišoft, P., Kalvová, J., and Brázdil, R.: Cycles and trends in the Czech temperature series using wavelet transforms, Int. J. Climatol., 24, 1661–1670, doi:10.1002/joc.1095, 2004.

Qi, J.: Odd phenomenon develops in used car market, do the “Yellow-label vehicles” restrictions work to mitigate air pollution, Xinhuanet, available at: http://news.xinhuanet.com/society/2010-11/28/c_12825457.htm (last access: 6 October 2015), 2010 (in Chinese).

Reuter, M., Buchwitz, M., Hilboll, A., Richter, A., Schneising, O., Hilker, M., Heymann, J., Bovensmann, H., and Burrows, J. P.: Decreasing emissions of NO_x relative to CO_2 in East

Asia inferred from satellite observations, Nat. Geosci., 7, 792–795, doi:10.1038/ngeo2257, 2014.

Richter, A., Burrows, J. P., Nusz, H., Granier, C., and Niemeier, U.: Increase in tropospheric nitrogen dioxide over China observed from space, Nature, 437, 129–132, doi:10.1038/nature04092, 2005.

Rienecker, M., Suarez, M., Todling, R., Bacmeister, J., Takacs, L., Liu, H., Gu, W., Sienkiewicz, M., Koster, R., and Gelaro, R.: The GEOS-5 Data Assimilation System-Documentation of Versions 5.0. 1, 5.1. 0, and 5.2. 0, NASA Tech. Memo 104606, 2008.

Russell, A. R., Valin, L. C., and Cohen, R. C.: Trends in OMI NO_2 observations over the United States: effects of emission control technology and the economic recession, Atmos. Chem. Phys., 12, 12197–12209, doi:10.5194/acp-12-12197-2012, 2012.

Shuai, S. and Zhongying, Q.: Energy development and economic growth in Western China: an empirical analysis based on the resource curse hypothesis (in Chinese), Economic Research Journal, 4, 147–160, 2008.

Stavrakou, T., Müller, J. F., Boersma, K. F., De Smedt, I., and van der A, R. J.: Assessing the distribution and growth rates of NO_x emission sources by inverting a 10 year record of NO_2 satellite columns, Geophys. Res. Lett., 35, L13801, doi:10.1029/2008GL033521, 2008.

The first nationwide pollution census committee: Pollution Census Dataset, China Environmental Science Press, 31–32, ISBN:9787511105356, 2011 (in Chinese).

The State Council of the People's Republic of China: Integrated Work Plan for Energy Saving and Emission Reduction During the Twelfth Five-Year Plan, available at: http://www.gov.cn/zwgk/2011-09/07/content_1941731.htm (last access: 10 June 2015), 2011a (in Chinese).

The State Council of the People's Republic of China: The Twelfth Five-Year Plan for Environmental Protection, available at: http://www.gov.cn/zwgk/2011-12/20/content_2024895.htm (last access: 10 June 2015), 2011b (in Chinese).

The State Council of the People's Republic of China: The Twelfth Five-Year Plan for Energy Saving and Emission Reduction, available at: http://www.gov.cn/zwgk/2012-08/21/content_2207867.htm (last access: 10 June 2015), 2012 (in Chinese).

Valin, L. C., Russell, A. R., Hudman, R. C., and Cohen, R. C.: Effects of model resolution on the interpretation of satellite NO_2 observations, Atmos. Chem. Phys., 11, 11647–11655, doi:10.5194/acp-11-11647-2011, 2011.

van der A, R. J., Peters, D. H. M. U., Eskes, H., Boersma, K. F., Van Roozendael, M., De Smedt, I., and Kelder, H. M.: Detection of the trend and seasonal variation in tropospheric NO_2 over China, J. Geophys. Res.-Atmos., 111, D12317, doi:10.1029/2005JD006594, 2006.

van der A, R. J., Eskes, H. J., Boersma, K. F., van Noije, T. P. C., Van Roozendael, M., De Smedt, I., Peters, D. H. M. U., and Meijer, E. W.: Trends, seasonal variability and dominant NO_x source derived from a ten year record of NO_2 measured from space, J. Geophys. Res.-Atmos., 113, D04302, doi:10.1029/2007JD009021, 2008.

Wang, S. and Hao, J.: Air quality management in China: issues, challenges, and options, J. Environ. Sci., 24, 2–13, doi:10.1016/S1001-0742(11)60724-9, 2012.

Wang, S. W., Zhang, Q., Streets, D. G., He, K. B., Martin, R. V., Lamsal, L. N., Chen, D., Lei, Y., and Lu, Z.: Growth in NO_x emissions from power plants in China: bottom-up estimates and satellite observations, Atmos. Chem. Phys., 12, 4429–4447, doi:10.5194/acp-12-4429-2012, 2012.

Wang, Y., McElroy, M. B., Boersma, K. F., Eskes, H. J., and Veefkind, J. P.: Traffic restrictions associated with the Sino–African summit: reductions of NO_x detected from space, Geophys. Res. Lett., 34, L08814, doi:10.1029/2007GL029326, 2007a.

Wang, Y., McElroy, M. B., Martin, R. V., Streets, D. G., Zhang, Q., and Fu, T.-M.: Seasonal variability of NO_x emissions over east China constrained by satellite observations: implications for combustion and microbial sources, J. Geophys. Res.-Atmos., 112, D06301, doi:10.1029/2006JD007538, 2007b.

Wang, Y., Hao, J., McElroy, M. B., Munger, J. W., Ma, H., Chen, D., and Nielsen, C. P.: Ozone air quality during the 2008 Beijing Olympics: effectiveness of emission restrictions, Atmos. Chem. Phys., 9, 5237–5251, doi:10.5194/acp-9-5237-2009, 2009.

Witte, J. C., Schoeberl, M. R., Douglass, A. R., Gleason, J. F., Krotkov, N. A., Gille, J. C., Pickering, K. E., and Livesey, N.: Satellite observations of changes in air quality during the 2008 Beijing Olympics and Paralympics, Geophys. Res. Lett., 36, L17803, doi:10.1029/2009GL039236, 2009.

Xu, Y., Yang, C.-J., and Xuan, X.: Engineering and optimization approaches to enhance the thermal efficiency of coal electricity generation in China, Energ. Policy, 60, 356–363, doi:10.1016/j.enpol.2013.05.047, 2013.

Zhang, Q., Streets, D. G., He, K., Wang, Y., Richter, A., Burrows, J. P., Uno, I., Jang, C. J., Chen, D., Yao, Z., and Lei, Y.: NO_x emission trends for China, 1995–2004: The view from the ground and the view from space, J. Geophys. Res.-Atmos., 112, D22306, doi:10.1029/2007JD008684, 2007a.

Zhang, Q., Streets, D. G., Carmichael, G. R., He, K. B., Huo, H., Kannari, A., Klimont, Z., Park, I. S., Reddy, S., Fu, J. S., Chen, D., Duan, L., Lei, Y., Wang, L. T., and Yao, Z. L.: Asian emissions in 2006 for the NASA INTEX-B mission, Atmos. Chem. Phys., 9, 5131–5153, doi:10.5194/acp-9-5131-2009, 2009a.

Zhang, Q., Streets, D. G., and He, K.: Satellite observations of recent power plant construction in Inner Mongolia, China, Geophys. Res. Lett., 36, L15809, doi:10.1029/2009GL038984, 2009b.

Zhang, Q., Geng, G., Wang, S., Richter, A., and He, K.: Satellite remote sensing of changes in NO_x emissions over China during 1996–2010, Chinese Sci. Bull., 57, 2857–2864, doi:10.1007/s11434-012-5015-4, 2012.

Zhang, X., Zhang, P., Zhang, Y., Li, X., and Qiu, H.: The trend, seasonal cycle, and sources of tropospheric NO_2 over China during 1997–2006 based on satellite measurement, Sci. China Ser. D, 50, 1877–1884, doi:10.1007/s11430-007-0141-6, 2007b.

Zhao, B., Wang, S. X., Liu, H., Xu, J. Y., Fu, K., Klimont, Z., Hao, J. M., He, K. B., Cofala, J., and Amann, M.: NO_x emissions in China: historical trends and future perspectives, Atmos. Chem. Phys., 13, 9869–9897, doi:10.5194/acp-13-9869-2013, 2013.

Zhao, C. and Wang, Y.: Assimilated inversion of NO_x emissions over east Asia using OMI NO_2 column measurements, Geophys. Res. Lett., 36, L06805, doi:10.1029/2008GL037123, 2009.

Zhao, H. Y., Zhang, Q., Guan, D. B., Davis, S. J., Liu, Z., Huo, H., Lin, J. T., Liu, W. D., and He, K. B.: Assessment of China's virtual air pollution transport embodied in trade by using a consumption-based emission inventory, Atmos. Chem. Phys., 15, 5443–5456, doi:10.5194/acp-15-5443-2015, 2015.

Table 1. Regional trends of OMI NO_2 VCDs over 2005–2013 and NO_x emission reduction plan of 2015.

	Region	Average NO_2 in 2005[a] 10^{15} molecules cm^{-2}	NO_2 trend[b] (% yr^{-1})	NO_x emission reduction plan of 2015 (%)[c]
Northwest	Gansu	0.9 (0.4, I)	7.5 ± 1.2	3.1
	Inner Mongolia	1.1 (0.4, I)	10.2 ± 1.3	5.8
	Ningxia	1.4 (0.4, I)	12.3 ± 1.7	4.9
	Qinghai	1.0 (0.5, II)	11.2 ± 1.2	−15.3
	Shaanxi	2.3 (0.5, II)	10.5 ± 1.0	9.9
	Xinjiang	1.0 (0.5, II)	15.1 ± 2.0	0
Southwest	Chongqing	2.2 (0.5, III)	7.8 ± 0.9	6.9
	Guangxi	1.2 (0.5, III)	4.0 ± 0.5	8.8
	Guizhou	1.3 (0.5, III)	6.9 ± 1.0	9.8
	Sichuan	1.7 (0.5, III)	6.1 ± 0.7	6.9
	Yunnan	0.7 (0.5, III)	4.2 ± 0.3	5.8
Region	West	1.3 (0.5, II)	8.6 ± 0.9	5.7
	Northwest	1.2 (0.5, II)	11.3 ± 1.0	4.5
	Southwest	1.4 (0.5, III)	5.9 ± 0.6	7.6
	BTH	9.2 (0.7, IV)	5.3 ± 0.8	13.9
	YRD	7.2 (1.2, V)	4.1 ± 0.6	17.7
	PRD	8.0 (1.2, VI)	−3.3 ± 0.3	16.9

[a] All the provincial NO_2 data have been subtracted by its respective "background" values. The "background" values and regions are indicated in the parentheses.

[b] NO_2 trends are derived from the *A5* time series. All trend values are relative to 2005 and are statistically significant.

[c] NO_x reduction represents the proposed emissions in 2015 relative to 2010. The value for PRD refers to the proposed target for Guangdong Province. Qinghai Province is allowed to emit more NO_x in 2015 compared to 2010.

Table 2. Linear regression for GEOS-Chem modeled annual mean NO_2 VCDs as a function of OMI values over China.

Year	2005	2006	2007	2008	2009	2010	2011	2012
Slope	1.11	1.18	1.19	1.09	1.15	1.17	1.26	1.22
Intercept	0.26	0.33	0.36	0.32	0.27	0.32	0.31	0.21
R^2	0.88	0.86	0.89	0.88	0.88	0.89	0.90	0.89

Table 3. Socioeconomic statistics for individual provinces and capital cities.

Region	Provincial regions	Urban population in 2005 (% of total)	Urban population in 2013 (% of total)	Industrial GDP annual growth rate for 2005–2013 (% yr^{-1})	Thermal power generation annual growth rate for 2005–2013 (% yr^{-1})	Hydropower generation annual growth rate for 2005–2013 (% yr^{-1})	Capital cities[*]	Increase in vehicle ownership between 2005 and 2012 (million vehicles)	Percentage of transportation to total NO_x emissions (%)
Northwest	Gansu	30.0	40.1	13.8	9.8	9.9	Lanzhou	–	21.1
	Inner Mongolia	47.2	58.7	20.3	16.9	15.0	Hohhot	0.41	17.5
	Ningxia	42.3	52.0	15.0	17.9	7.2	Yinchuan	0.18	21.3
	Qinghai	39.3	48.5	16.0	12.0	13.2	Xining	0.03	27
	Shaanxi	37.2	51.3	17.0	14.0	4.7	Xi'an	1.09	56.6
	Xinjiang	37.2	44.5	12.4	22.8	18.4	Urumqi	0.37	25.7
Southwest	Chongqing	45.2	58.3	19.4	11.2	14.5	Chongqing	2.79	40.9
	Guangxi	33.6	44.8	17.4	14.9	11.2	Nanning	0.6	47.7
	Guizhou	26.9	37.8	14.0	9.9	8.9	Guiyang	0.44	26.4
	Sichuan	33.0	44.9	18.5	6.0	15.4	Chengdu	1.56	46.9
	Yunnan	29.5	40.5	14.6	7.0	21.6	Kunming	1.02	34.1

[*] Vehicle data for Lanzhou are unavailable.

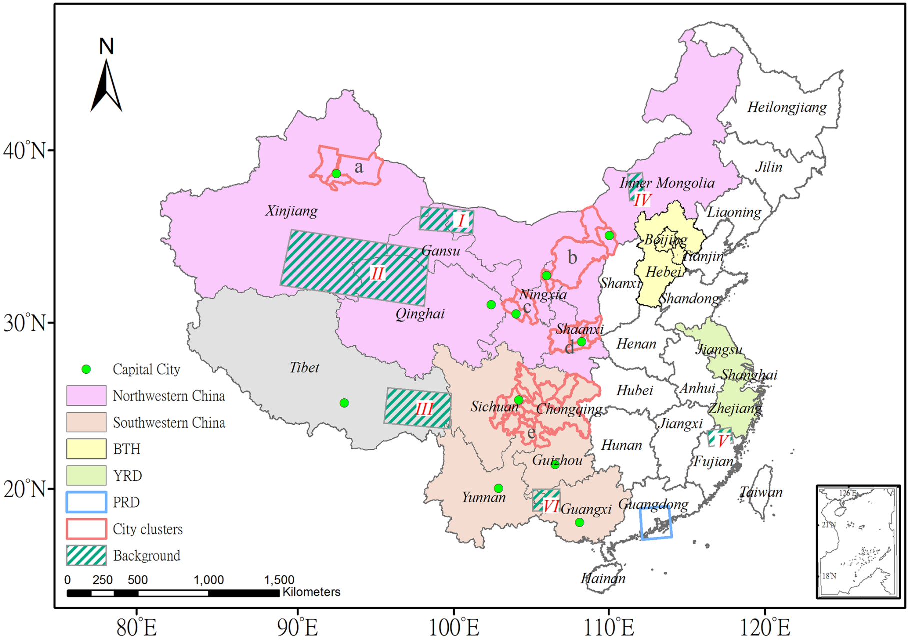

Figure 1. The study regions. Several city clusters are also identified: **(a)** Urumqi city cluster, **(b)** Inner Mongolia industrial city cluster, **(c)** Gansu-Ningxia, **(d)** Shaanxi-Guanzhong, and **(e)** Chengdu-Chongqing.

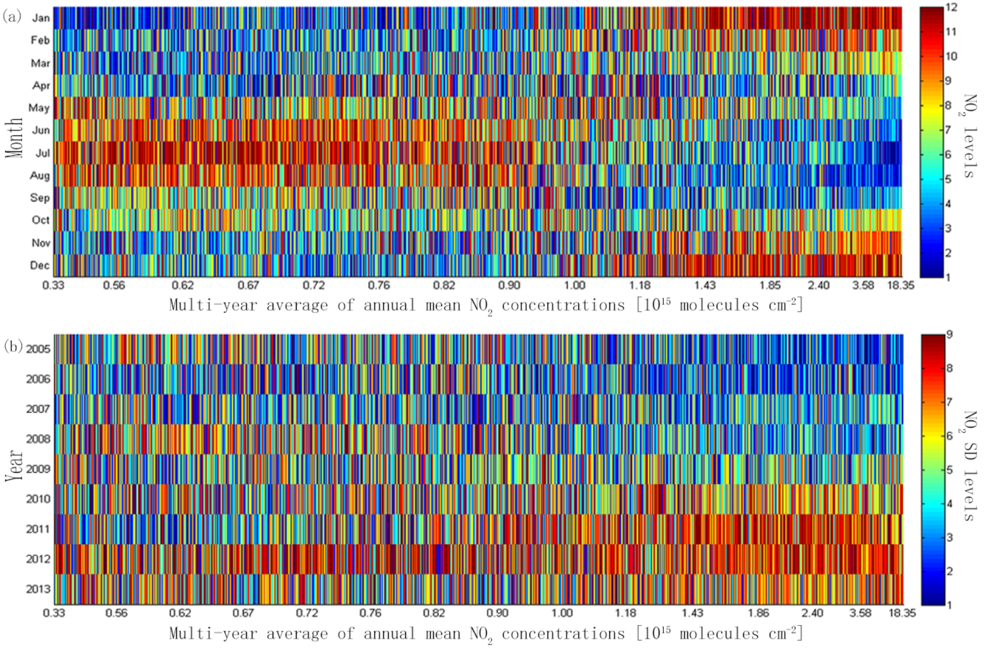

Figure 2. (a) 2005–2013 average seasonal variation of OMI NO_2 VCDs for each 0.25° × 0.25° grid cell of Western China; the grid cell is sorted by its 9 year average NO_2 VCD. For each grid cell, the 9 year average monthly NO_2 values are converted to their reverse ranks (from 1 to 12; 1 represents the smallest NO_2 value). **(b)** Standard deviation (SD) of monthly OMI NO_2 VCDs in individual years over 2005–2013 for each 0.25° × 0.25° grid cell of Western China; the grid cell is sorted by its 9 year average NO_2VCD. For each grid cell, the seasonal SDs in the nine years are converted to their reverse ranks (from 1 to 9; 1 represents the smallest SD value).

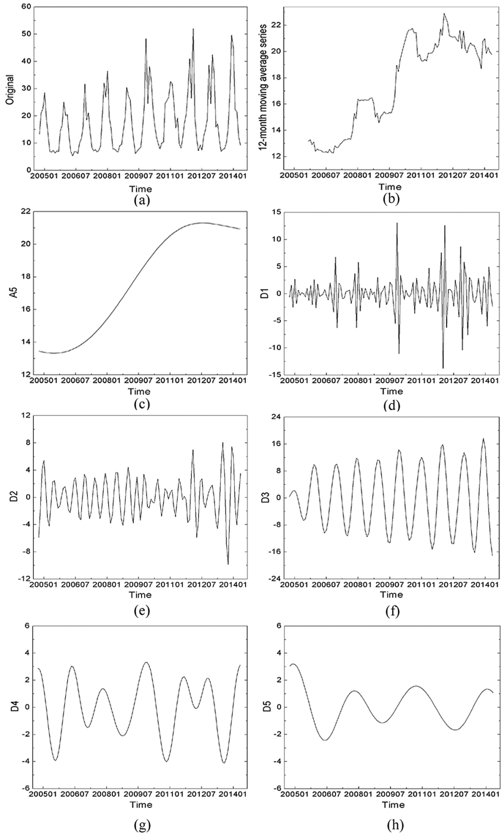

Figure 3. An example of the 5-level wavelet decomposition. **(a)** The original monthly time series of OMI NO_2 at a grid cell in Xi'an (34.5° N, 108.9° E), **(b)** The 12 month moving average time series, **(c)** The approximate signal *A5* representing the long-term trend, **(d–h)** Five decomposition levels *D1–D5* indicating temporal variability at various scales. In particular, *D3* represents the seasonality.

Title Page

Abstract | Introduction

Conclusions | References

Tables | Figures

◀| |▶

◀ ▶

Back | Close

Full Screen / Esc

Printer-friendly Version

Interactive Discussion

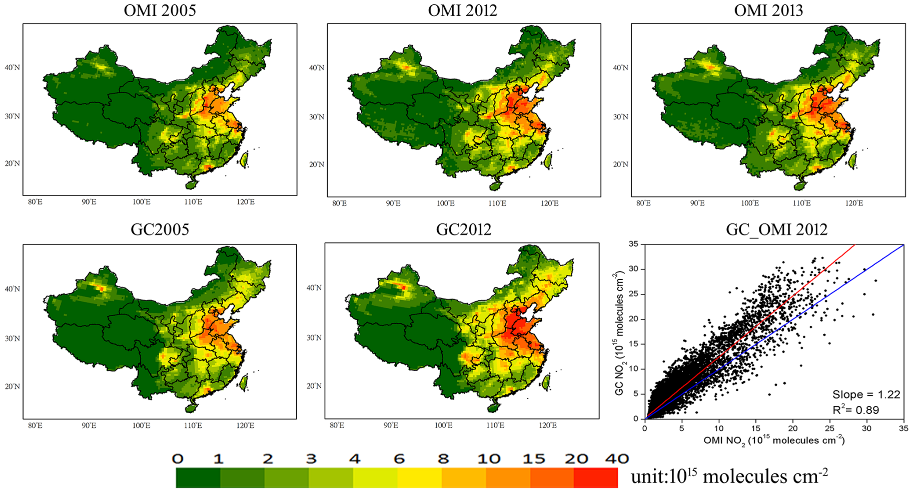

Figure 4. Annual mean OMI NO_2 VCDs over China in 2005, 2012 and 2013, annual mean GEOS-Chem NO_2 VCDs in 2005 and 2012, and a scatterplot with linear regression for model vs. OMI NO_2 in 2012.

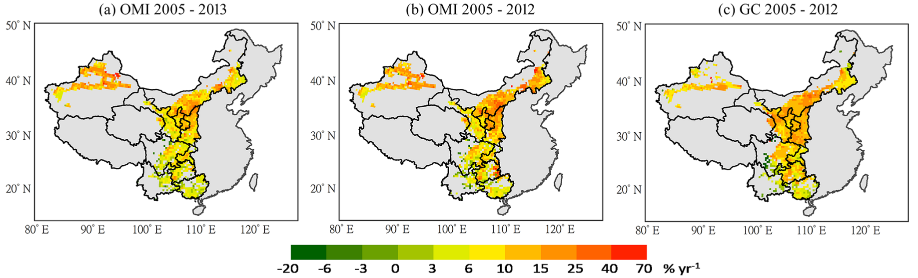

Figure 5. Percentage trends of annual mean OMI and Model NO_2 VCDs over Western China (relative to 2005), by applying a linear regression to the approximate signal *A5* from the wavelet decomposition. All the NO_2 data have been subtracted by its respective "background" values prior to the wavelet decomposition. Results are shown only for grid cells with 2005–2013 average NO_2 VCDs exceeding 1.0×10^{15} molecules cm^{-2} and with statistically significant trends (P value < 0.05 according to an F test). **(a)** OMI NO_2 trends from 2005 to 2013, **(b)** OMI NO_2 trends from 2005 to 2012, **(c)** Model NO_2 trends from 2005 to 2012.

Title Page
Abstract | Introduction
Conclusions | References
Tables | Figures
◀| |▶
◀ ▶
Back | Close
Full Screen / Esc
Printer-friendly Version
Interactive Discussion

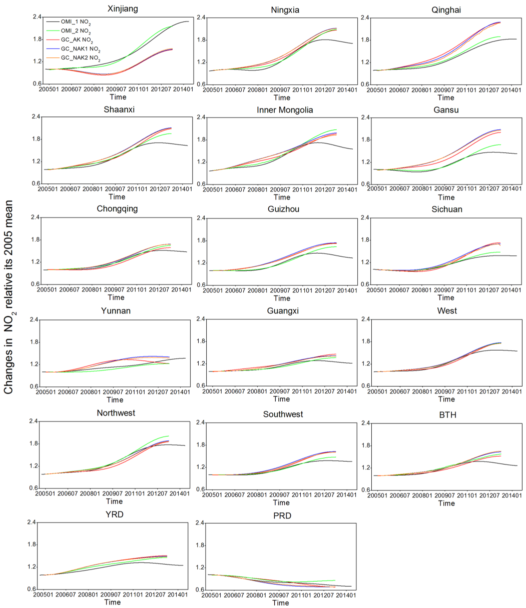

Figure 6. The long-term trends (i.e., the *A5* component out of the wavelet analysis) of OMI and modeled NO$_2$ in individual provinces and regions. The values are normalized to 2005. OMI_1 (black line) denotes the *A5* signal from a wavelet analysis of OMI NO$_2$ over October 2004–May 2014, and OMI_2 (green line) corresponds to the wavelet analysis over January 2005–April 2013. GC_AK (red line) corresponds to a wavelet analysis of coincident modeled values (applied with the AK) over January 2005–April 2013. GC_NAK1 (blue line) represents the *A5* signal for modeled NO$_2$ in all days (without applying the AK) over January 2005–April 2013, and GC_NAK2 (orange line) is similar to GC_NAK1 but with model results coincident with valid OMI data.

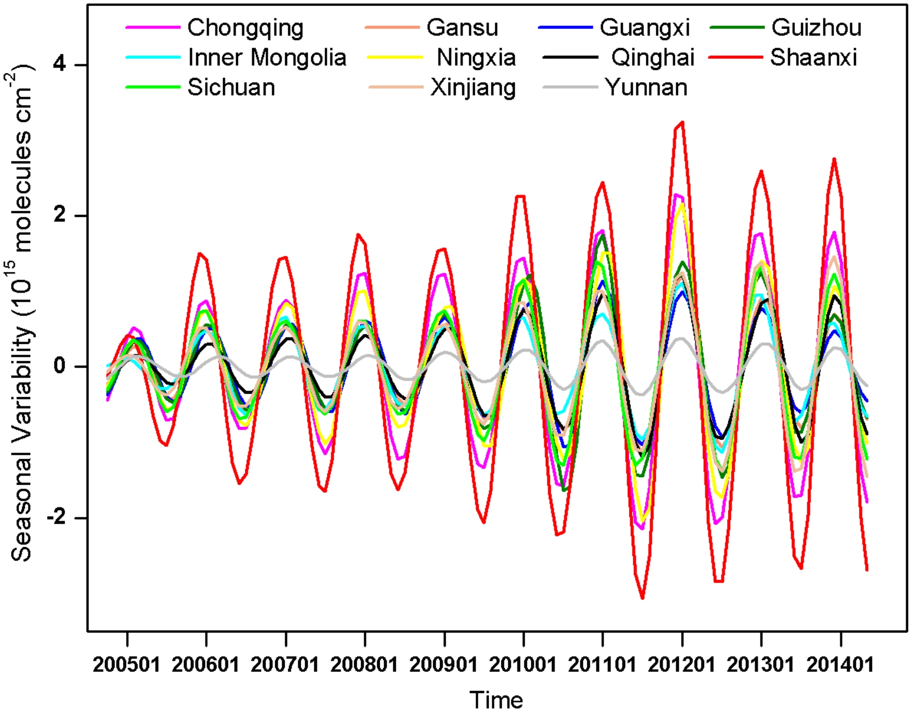

Figure 7. The seasonality component (*D3*) out of the wavelet analysis on monthly OMI NO_2.

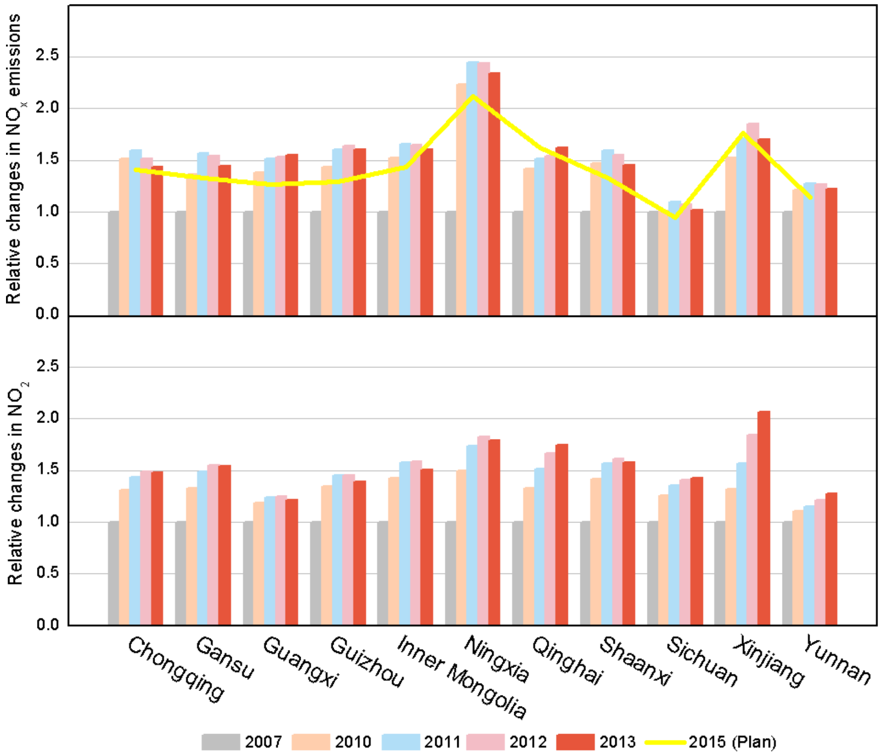

Figure 8. Relative Changes in OMI NO_2 VCDs and NO_x emissions in 2007 and 2010–2013 (relative to 2007). (Top) Chinese official provincial-level NO_x emission inventory for 2007 and 2010–2013 as well as its targeted emissions for 2015. (Bottom) Annual mean OMI NO_2 levels in 2007 and 2010–2013.

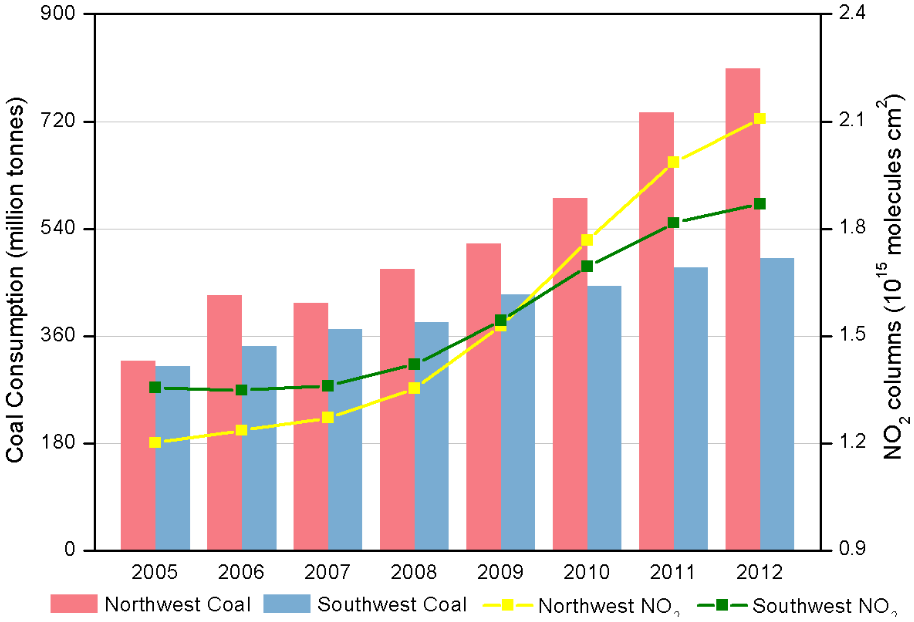

Figure 9. Coal consumption and annual mean OMI NO$_2$ levels over Western China.